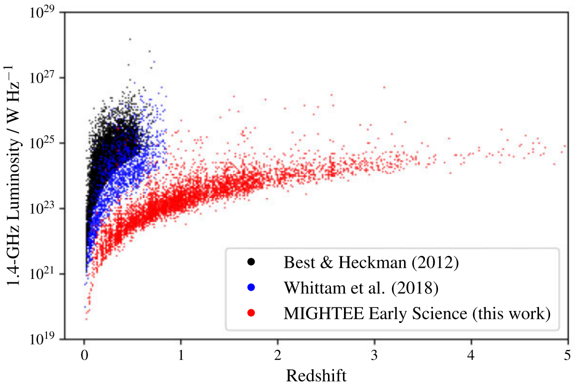

Figure 1. 1.4-GHz radio luminosity and redshift of the MIGHTEE Early Science multiwavelength cross-matched sample presented by Prescott et al. (in preparation) and studied in this work (red), along with the samples studied by Best & Heckman (2012) (black) and Whittam et al. (2018) (blue).

(2022) shows that the link between accretion mode and morphology is very indirect. There is also evidence that HERGs seem to be more dominated by radio emission from their cores than LERGs (Whittam et al. 2016).

It had been proposed that there is a direct relationship between the accretion mode and the source of fuel available, with HERGs accreting efficiently from sources of cold gas, while LERGs accrete inefficiently from the hot gas halo (Hardcastle, Evans & Croston 2007). More recent work, however, has argued that Eddington-scaled accretion rate is the key driver of the difference between HERGs and LERGs, rather than the source of the material being accreted (e.g. Best & Heckman 2012; Best et al. 2014; Hardcastle 2018; Hardcastle & Croston 2020). It is therefore important that we fully understand the Eddington-scaled accretion rates of different AGN classes as we probe lower radio powers and higher redshifts.

In the scenario building up in the literature, there has been thought to be a dichotomy in accretion rates between the HERG and LERG classes; HERGs accrete efficiently at $\gtrsim$1 per cent of their Eddington accretion rate, while LERGs accrete much more slowly at $\lesssim$1 per cent of Eddington, with almost no overlap in the accretion rates of the two classes (Best & Heckman 2012; Mingo et al. 2014). The current understanding is that this is because the two classes are a result of two fundamentally distinct accretion modes (Best et al. 2005; Hardcastle, Evans & Croston 2006). HERGs are thought to accrete cold gas efficiently via an optically thick, geometrically thin accretion disc (e.g. Shakura & Sunyaev 1973), while LERGs accrete from a hot gas reservoir (e.g. Hardcastle et al. 2007; Janssen et al. 2012; Yuan & Narayan 2014) relatively slowly via an advection-dominated accretion flow (Narayan & Yi 1995; Quataert 2003).

However, recent work by Whittam et al. (2018) using radio galaxies selected from a Karl G. Jansky Very Large Array (VLA) survey of Stripe-82 (Heywood et al. 2016) has suggested that the dichotomy in accretion rates of HERGs and LERGs may not be as clear cut as previously thought; Whittam et al. find a significant overlap in the accretion rates of the two classes. The Whittam et al. study probes lower radio luminosities than the Best & Heckman (2012) work (see Fig. 1) and the Mingo et al. (2014) study; this may be the reason for the larger overlap in accretion rates, but Whittam et al. do not have the statistics at lower luminosities to confirm this trend.

This suggests that the current leading model where there are two distinct accretion modes, which equate to different feedback processes (see review by Fabian 2012), does not tell the full story, and instead galaxies may display a more continuous range of accretion rates and associated properties. This has important implications for our understanding of galaxy evolution and how AGN processes affect star formation in a galaxy (e.g. Cattaneo et al. 2009; Hardcastle & Croston 2020). However, further research at lower radio luminosities is required to confirm this, which is the aim of this work.

The MeerKAT International Tiered GHz Extragalactic Exploration (MIGHTEE; Jarvis et al. 2016) survey is a large survey project currently underway with the MeerKAT radio telescope (Jonas 2009). When complete, MIGHTEE will cover 20 deg^2 across four different fields (COSMOS, XMM-LSS, ELAIS-S1, and E-CDFS) to a depth of $\sim$ 2 μJy per beam rms at 1.28 GHz. The unique combination of depth over a significant area combined with excellent multiwavelength coverage means that the MIGHTEE survey has the potential to provide a significant step forward in our understanding of galaxy evolution. In particular, the MIGHTEE survey allows us to study the accretion rates of a large sample of AGNs across a range of radio powers and redshifts. In this paper, we use MIGHTEE Early Science observations in the COSMOS field (Heywood et al. 2022) to probe the nature of the apparently faint radio source population, focusing on the properties of RLAGNs.

This paper is laid out as follows: in Section 2, we describe the MIGHTEE radio data used in this work, and the ancillary multiwavelength data used are outlined in Section 3. In Section 4, we explain the scheme used to classify the MIGHTEE radio sources. We then use this sample to explore the properties of RLAGN in Section 5; first we discuss the host galaxy properties of different types of RLAGNs, next we investigate the accretion rates of these classes, then we explore the host galaxy properties as a function of accretion rate, and finally we discuss the relationship between AGN power and black hole mass. The implications of these results are discussed in Section 6, and our conclusions are presented in Section 7.

Throughout this paper, the following values for the cosmological parameters are used: $H_0 = 70$ km s^{-1} Mpc^{-1}, $\Omega_{\rm M} = 0.3$, and $\Omega_\Lambda = 0.7$. Unless stated, all magnitudes are AB magnitudes. We use the following convention for radio spectral index, α: $S \propto \nu^{-\alpha}$, for a source with flux density S and frequency ν.

2 RADIO DATA – THE MIGHTEE SURVEY

The MIGHTEE Early Science radio continuum data release consists of one pointing in the COSMOS field, covering $\sim$1.6 deg^2, and three overlapping pointings in the *XMM*-LSS field, covering $\sim$3.5 deg^2. In this work, we restrict our analysis to the central part of the COSMOS Early Science image, with a diameter of 1.04 deg, as this is the region over which multiwavelength counterparts for the radio sources have been identified (see Section 3.2 and Prescott et al., in preparation). These observations consist of a single field of view with the MeerKAT telescope centred on RA 10h00m28.6s, Dec. +02d12m21s. The observations were taken with the *L*-band receiver (bandwidth 900–1670 MHz) between 2018 and 2020 and include 17.45 h on source. For full details of the observations and data reduction, we refer the reader to Heywood et al. (2022).

The MIGHTEE Early Science data contains two versions of the data processed with different Briggs (1995) robust weighting values; the first uses Briggs' robustness parameter = 0.0 and is optimized for sensitivity but has lower resolution. The second image uses robust = -1.2 which downweights the short baselines in the core resulting in a higher resolution but this comes at the expense of sensitivity. In this paper, we use the maximum-sensitivity (robust = 0.0) image, which has a circular synthesized beam full width at half-maximum

(FWHM) diameter of 8.6 arcsec and a thermal noise of 1.7 μJy per beam. However, due to confusion noise the effective rms noise in the centre of the image is ∼ 4 μJy per beam (Heywood et al. 2022).

Source finding was carried out using the PYTHON Blob Detector and Source Finder (PYBDSF; Mohan & Rafferty 2015) using the default source extract parameters (see Heywood et al. 2022 for further details). Our initial sample contains 6263 radio sources with $S_{1.28\ \mathrm{GHz}} > 20\mu$Jy in the central part of the COSMOS field.[1] As mentioned, the full MIGHTEE Early Science data released by Heywood et al. covers a larger area of the COSMOS field as well as the *XMM*-LSS field, so contains a much larger number of sources, but here we are limited to the region over which the multiwavelength counterparts for the radio sources have been identified to date.

Due to the wide bandwidth of the MeerKAT *L*-band receivers used for the MIGHTEE observations (900–1670 MHz) and the varying response of the primary beam with frequency (together with other factors such as flagging of the raw data), the effective frequency of the MIGHTEE data varies across the image. This is discussed in detail in Heywood et al. (2022). In order to have measurements at a constant frequency and to aid comparisons with other work, we scale the MIGHTEE flux densities and radio luminosities to 1.4 GHz using the effective frequency map released with Heywood et al., assuming a spectral index of 0.7. All radio luminosities are *k*-corrected assuming the same spectral index.

Due to the depth of the radio data used to select the sample studied in this paper, together with the quality of the ancillary data (see Section 3), we are able to probe lower radio luminosities and higher redshifts than previous studies of the accretion rates of RLAGNs, such as Best & Heckman (2012) and Whittam et al. (2018). This is illustrated by Fig. 1 which shows the radio luminosity and redshift distribution probed by this work compared to those of two previous studies. As can been seen in the figure, there is almost no overlap in the parameter space probed by the MIGHTEE sample and the Best & Heckman (2012) study. This demonstrates the unique power of the MIGHTEE survey to probe low-powered radio galaxies across cosmic time, which therefore has potential to provide a new insight into AGN activity.

3 MULTIWAVELENGTH DATA

3.1 Optical and near-infrared

This work makes use of the extensive optical and near-infrared data in the COSMOS field compiled by Bowler et al. (2020; see also Adams et al. 2020, 2021). Briefly, this contains near-infrared imaging in the $YJHK_s$ band from the fourth data release (DR4) of the UltraVISTA survey (McCracken et al. 2012), optical data in *grizy* filters from Hyper Suprime-Cam Subaru Strategic Program DR1 (HSC SSP; Tanaka et al. 2017) along with data from two HSC narrow-band filters at 8160 and 9210 Å, deeper optical imaging in the u^*griz filters from the Canada–France–Hawaii Telescope Legacy Survey (CFHTLS), and deep z'-band imaging from Subaru/Suprime-Cam (Furusawa et al. 2016). Additionally, mid-infrared data from the *Spitzer* Infrared Array Camera (IRAC) at 3.6 and 4.5 μm is included. This combines shallower imaging from the *Spitzer* Large-Area Survey with the HSC (SPLASH; Steinhardt et al. 2014) with deeper data from the *Spitzer* Matching Survey of the UltraVISTA ultradeep Stripes survey (SMUVS; Ashby et al. 2018) and the *Spitzer* Extended Deep Survey (SEDS; Ashby et al. 2013). Full details of the catalogue creation are given in Bowler et al. (2020).

Additionally, this work makes use of the high-resolution *Hubble Space Telesope (HST)* Advanced Camera for Surveys (ACS) *I*-band image (further details of these data are given in Scoville et al. 2007).

3.2 Cross-matching

The procedure used to identify the host galaxy of each radio source is described in detail in Prescott et al. (in preparation) and summarized briefly here. Overlays displaying the MIGHTEE radio contours and the higher resolution Smolčić et al. (2017a) VLA-COSMOS 3 GHz radio contours on top of the UltraVISTA K_s-band images were produced for each MIGHTEE radio component in the early science low resolution Level 0 catalogue (described in Heywood et al.). Although less sensitive for a typical radio source with a spectral index of 0.7 (median rms is $S_{3\ \mathrm{GHz}} \sim 2.3$ μJy per beam), the higher resolution (0.78 arcsec) VLA-COSMOS 3 GHz data are useful when identifying the correct host galaxy for the radio sources.

Prescott et al. (in preparation) use an updated version of the XMATCHIT code (described in Prescott et al. 2018) to quickly display the overlays for each radio component. These were examined by eye by three separate people to identify the most likely host galaxy for each radio component. Any sources where the three classifiers did not agree were examined again by a committee. In total, we have identified the host galaxy for 5223 out of 6262 (83 per cent) radio sources. The 1039 unmatched radio sources are a combination of sources which lie in masked regions close to bright sources in the K_s-band image (208 sources), sources which are too confused for us to be able to identify the correct host ID (i.e. where two or more individual sources with separate host galaxies are blended together in the radio image; 693 sources), sources where there is no host galaxy visible in the UltraVISTA K_s-band image (126 sources), and sources which appear to be artefacts in the radio image (12 sources; note that these do not appear in the MIGHTEE Early Science Level 1 catalogue released by Heywood et al. where artefacts have been removed). This is discussed further in Prescott et al. (in preparation). This sample of 5223 sources is the focus of the remainder of this paper.

3.3 Mid and far-infrared

In addition to the data from the two shorter wavelength *Spitzer* IRAC bands included in the Bowler et al. (2020) compilation described in Section 3.1, we use data from the 5.8 and 8.0 μm bands from the SPLASH survey, accessed from Laigle et al. (2016).

Far-infrared data were obtained from the *Herschel* Extra-galactic Legacy Project (HELP; Shirley et al. 2021). We use data at 24 μm from the Multiband Imaging Photometer (MIPS; Rieke et al. 2004) instrument on the *Spitzer* Space Telescope, 100 and 160 μm from the Photodetector Array Camera and Spectrometer (PACS; Poglitsch et al. 2010) on *Herschel* and 250, 350, and 500 μm from the Spectral and Photometric Imaging Receiver (SPIRE; Griffin et al. 2010), also on *Herschel*. Photometry was obtained using XID+ (Hurley et al. 2017), a probabilistic de-blender developed for the HELP project. This utilizes prior information from the four *Spitzer* IRAC bands, which have a higher resolution than the *Herschel* data, and applies a Bayesian approach to extract photometry from the *Herschel* maps.

The HELP far-infrared catalogues were combined with the cross-matched catalogue (Section 3.2) by matching to the position of the host galaxy using a match radius of 1 arcsec. 4540 out of 5223 radio

[1]Note that components which make up part of an extended radio source are grouped together as part of the cross-matching process described in Section 3.2